JOURNAL OF GEOPHYSICAL RESEARCH, VOL. 103, NO. C10, PAGES 21,469–21,479, SEPTEMBER 15, 1998

Energy conversion in the Cape Verde Frontal Zone

Wolfgang Erasmi, Gerold Siedler, and Reiner Onken[1]
Institut für Meereskunde, Kiel, Germany

Abstract. Mechanical energy terms are calculated from moored current meter data in the Cape Verde Frontal Zone (about 20°N, 25°W) and compared with those derived from a mesoscale model of this frontal region. The model is of the *Bleck and Boudra* [1981] type with isopycnal coordinates. An initially zonal jet, representing the Canary Current, is allowed to develop under the influence of baroclinic and barotropic instability processes. We find reasonable agreement in magnitudes, somewhat smaller in the model, and similar distributions in the vertical. This leads to the conclusion that the energy transfer terms from the model can be expected to be sufficiently close to reality. Determination of the transfer terms confirms that the energy transfer in the zone is dominated by baroclinic instability processes while barotropic instability is of minor importance. Average baroclinic instability energy transfer terms reach values of 2–3 μW m^{-3} in the pycnocline. Peak layer mean values are of the order 10 μW m^{-3}. It is shown that the spatial distribution of active transfer regions is closely related to the structure of the transient eddy field in the frontal zone and that strong instability processes are restricted to the pycnocline.

1. Introduction

The Cape Verde Frontal Zone forms the southeastern boundary of the North Atlantic subtropical gyre (Figure 1). A significant part of the recirculation is found here in the Canary Current, arriving from the north and being transformed into the westward flowing North Equatorial Current.

In the main thermocline, relatively warm and haline North Atlantic Central Water in the northwest is opposed to colder and fresher South Atlantic Central Water in the southeast. The front between the two types of central water extends from southwest to northeast in this region, which is different from its generally zonal orientation in the open ocean [*Tomczak*, 1984].

Since earlier studies were conducted [*Barton*, 1987; *Tomczak and Hughes*, 1980; *Tomczak*, 1981], the Cape Verde Frontal Zone has been the subject of intensive observations. The measurements provide details of the water mass structure [*Fiekas et al.*, 1992; *Klein and Siedler*, 1995] and evidence of strong oceanic fronts with meandering and mesoscale activity [*Zenk et al.*, 1991; *Klein and Siedler*, 1995]. Efforts have been made to determine timescales and energy partition in the region [*Onken and Klein*, 1991].

Various model studies have provided results, including the Central Water Boundary [e.g., *Cox*, 1985; *Spall*, 1990, 1992; *Treguier*, 1992; *Spall et al.*, 1993; *Beckmann et al.*, 1994], or were specifically aimed at this particular front [*Onken and Klein*, 1991]. In the present study we intend to provide some further insight into the processes that control the energy of the flow in the Cape Verde Frontal Zone and to obtain quantitative estimates. We compare mechanical energy terms from observations and from a model for the frontal region, and we determine the rates of conversion between the mean and eddy kinetic energies and the potential energy from the model.

[1]Now at SACLANT Undersea Research Centre, La Spezia, Italy.

Paper number 98JC01887.
0148-0227/98/98JC-01887$09.00

2. Energy and Transfer Terms

Using the relation $X = \bar{X} + X'$ for a variable X with a time mean value $\bar{X}$ and a fluctuation X', one obtains the terms for mean kinetic energy (MKE), eddy kinetic energy (EKE), mean potential energy (MPE), and eddy potential energy (EPE) [cf. *Oort et al.*, 1989]:

$$\mathrm{MPE} = -\frac{g}{2}\frac{(\bar{\rho} - \tilde{\rho})^2}{\partial\tilde{\rho}/\partial z} \tag{1}$$

$$\mathrm{EPE} = -\frac{g}{2}\frac{\overline{\rho'^2}}{\partial\tilde{\rho}/\partial z} \tag{2}$$

$$\mathrm{MKE} = \rho_0\frac{\bar{u}^2 + \bar{v}^2}{2} \tag{3}$$

$$\mathrm{EKE} = \rho_0\frac{\overline{u'^2 + v'^2}}{2} \tag{4}$$

Here g is the acceleration of gravity; u, v, and w are the components of velocity in directions x, y, and z, respectively; and ρ denotes density. Also, $\tilde{\rho} = \tilde{\rho}(z)$ is the global mean density on a depth level z as a reference state for available potential energy [see *Lorenz*, 1955; *Reid et al.*, 1981], while ρ_0 describes the average density of seawater. The assumption is made that $\rho' \ll \rho$, $\bar{\rho}$ and $w \ll u$, v. For details, see *Oort et al.* [1989].

The terms for energy conversion can be found by constructing equations for the time derivatives of the energy terms [*Orlanski and Cox*, 1973; *Harrison and Robinson*, 1978]. The energy conversion terms read

$$C(\mathrm{MPE, EPE}) = \frac{g}{\partial\tilde{\rho}/\partial z}\left(\overline{u'\rho'}\frac{\partial\bar{\rho}}{\partial x} + \overline{v'\rho'}\frac{\partial\bar{\rho}}{\partial y}\right) \tag{5}$$

$$C(\mathrm{MKE, EKE}) = -\rho_0\left[\overline{u'u'}\frac{\partial\bar{u}}{\partial x} + \overline{v'v'}\frac{\partial\bar{v}}{\partial y} + \overline{u'v'}\left(\frac{\partial\bar{u}}{\partial y} + \frac{\partial\bar{u}}{\partial x}\right)\right] \tag{6}$$

$$C(\mathrm{MPE, MKE}) = -g\overline{w\rho} \tag{7}$$

$$C(\mathrm{EPE, EKE}) = -g\overline{w'\rho'} \tag{8}$$

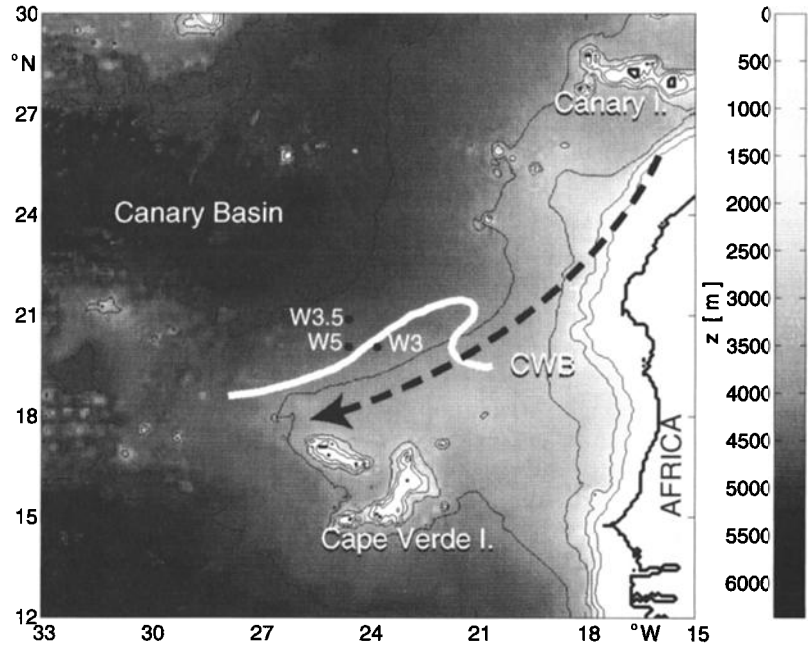

Figure 1. The Cape Verde Frontal Zone off the West African coast. The 1000- to 5000-m isobaths are indicated by solid lines. The white line represents the Central Water Boundary (CWB) as found by *Zenk et al.* [1991]. The approximate path of the Canary Current is sketched by the dashed line, according to *Siedler and Onken* [1996]. The positions of three moorings (W3, W3.5, and W5) deployed in 1989 are indicated by black dots.

The terminology of *Bleck* [1985] is used here for C; that is, a positive value for C(A,B) means conversion of energy of type A into that of type B. An analogous set of equations derived by *Bleck* [1985] for isopycnal coordinate systems is applied in the model in the same form as that used by *Bleck and Boudra* [1986], who avoided distinguishing between mean and eddy potential energy in the conversion, considering only their sum as potential energy (PE). Such a division is unnecessary as long as energy conversions are considered in order to identify the physical mechanism of instability. For more details, see *Bleck* [1985] or *Boudra et al.* [1988].

For the purpose of studying the time development of the energy conversion in the model, the terms are used also as momentary (not yet time averaged) quantities. In this case they are denoted by (lower case) c(A,B). In addition, it is worth mentioning that at any instant the temporal mean (denoted by the overbar in (1)–(8)) is evaluated over the preceding period of time, hence it changes with time in the calculations from observations and in the model as well.

3. Observational database

Multiyear time series were obtained from current meter moorings in the 1980s [*Müller and Siedler*, 1992], and hydrographic sections were carried out in several consecutive years [*Müller et al.*, 1988; *Siedler et al.*, 1987; *Zenk et al.*, 1989]. We use the most recent current velocity data, collected by a triangular array of moorings (W3, W3.5, and W5) placed in the Central Water Boundary in 1989 [*Zenk et al.*, 1989]. The positions of these moorings are given in Table 1 and Figure 1.

Two of these moorings were part of a previously deployed chain of moorings crossing the Central Water Boundary, which determined the horizontal distances between the moorings. Since these are larger than the local Rossby radius of deformation (≈50 km in this area), the fluctuations of properties are likely to be incoherent [*Spall*, 1990; *Emery et al.*, 1984] and cannot be used for the calculation of energy transfers. The mooring data will, however, provide estimates of the energy terms for the region.

4. Model

We use a Bleck and Boudra type isopycnic primitive equation model [*Bleck*, 1978; *Bleck and Boudra*, 1981] as adapted by *Onken and Klein* [1991] for their study of the instability of the Canary Current. It spans an area of 1000 km × 1000 km on 64 × 64 grid points and 11 layers of constant potential density in the vertical. Bottom depth is variable in the cross-frontal

Table 1. Positions and Operational Times of Mooring Array W3, W3.5, and W5

Mooring	Number	Latitude, N	Longitude, W	Depth, m	Date Deployed in 1989	Date Exchanged in 1989	Date Recovered in 1990
313-3/4	W3	20°25.6′	023°38.4′	4520	Jan. 21	Oct. 31	Sept. 29
320-1/2	W3.5	21°13.0′	024°25.4′	4958	Jan. 19	Oct. 30	Sept. 27
314-2/3	W5	20°25.8′	024°25.6′	4702	Jan. 20	Nov. 1	Sept. 30

direction and constant along the front, representing the simplified Cape Verde Plateau (Figure 2). The properties of the vertical layers are given in Table 2.

In order to simulate the Canary Current, which flows from northeast to southwest, the model channel should be rotated by about 45° from the east-west orientation. Since the model uses periodic boundary conditions, however, we instead reduce the β term in the model by a factor of cos(45°):

$$f = f_0 + \beta(y - B/2)\cos(45°) \quad (9)$$

Here f is the Coriolis parameter, f_0 is the Coriolis parameter at reference latitude (20°N), $\beta \equiv \partial f/\partial y$ denotes the variation of f in the meridional direction, and B is the channel width. In this way, f varies by the same amount in the cross-frontal direction in the model as it does in nature. The coordinates x and y are referred to as "along-channel" and "cross-channel" coordinates, respectively, rather than "zonal" and "meridional."

Model initialization is made by fitting the initial density and temperature fields to a representative cross-frontal conductivity-temperature-depth (CTD) section [*Zenk et al.*, 1991] while conserving isopycnal potential vorticity. The isopycnal slope corresponds to a geostrophically balanced initial jet that may be interpreted as the undisturbed Canary Current. After superimposing small disturbances to the jet, the model is run without external forcing, subject to internal friction only. In our particular experiment the total run time is 700 days. During this time the total energy in the system decreases to 77% of the initial value, and the total model run time is therefore considered sufficiently short for a study of energy and conversion terms. As shown in section 6.1, the model has an initial spin-up period of 180 to 200 days. Within the model run time from days 200 to 700, the nature of the processes did not seem to vary considerably. We therefore accepted this to be an appropriate averaging period for the determination of the presented properties. For details of the model, refer to *Onken and Klein* [1991] and *Bleck and Boudra* [1981].

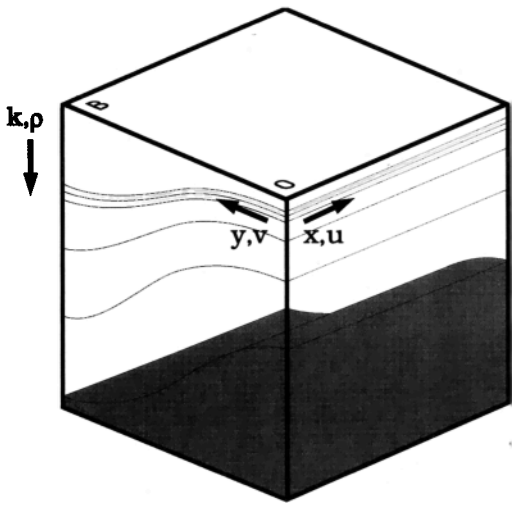

Figure 2. Schematics of the model domain, where x is the along-channel coordinate, y is the cross-channel coordinate, ρ is the vertical coordinate, and k is the index of density layers. Between surface and bottom are density layer schematics drawn as an example.

Table 2. Potential Density Anomaly σ_θ of Model Layers

Layer Number k	σ_θ, kg m^{-3}	h_{min}, m	h_{mean}, m	h_{max}, m
1	24.95	32.8	44.8	54.7
2	25.25	34.8	49.5	61.6
3	25.55	36.8	53.6	67.6
4	25.85	40.8	64.7	84.5
5	26.15	50.7	87.1	117.4
6	26.45	88.5	155.3	210.8
7	26.75	245.8	301.8	349.0
8	27.05	531.8	555.2	576.9
9	27.35	958.5	933.3	910.3
10	27.65	1664.0	1606.8	1554.1
11	27.95	3044.6	4327.6	5423.5

Values h_{min}, h_{mean}, and h_{max} denote the minimum, mean, and maximum lower interface depth, respectively, of each layer.

5. Energy Terms

We first present the results from the current meter observations. An analysis of the velocity data using cumulative averaging showed that the time series obtained from moorings W3, W3.5, and W5 were long enough to obtain stable mean values for the derivation of the energy terms MKE and EKE. The only exceptions are the records from the current meters at the 400-m level of W3 and W5 and the 1200-m level of W3.5. Table 3 provides statistical data from the current meter records.

Mean velocities are low, and the flow is dominated by fluctuations. The mean eastward and northward velocity components in the upper 400 m have maximum values of 0.026 m s^{-1} but are not significantly different from zero. The variances $\overline{u'^2}$ and $\overline{v'^2}$ have a range from 0.8×10^{-3} to 4.52×10^{-3} m^2 s^{-2}. The magnitude of eddy kinetic energy varies between 1.28 and 3.84 J m^{-3} in this depth range.

Since the signals of the three moorings are incoherent, the time series of all instruments of one depth may be combined in ensembles. Weighted means of kinetic energy terms are calculated. The results are shown in Figure 3. At each depth level the fluctuating part of kinetic energy dominates the mean kinetic energy by at least 1 order of magnitude. EKE values decrease from 3.6 J m^{-3} at about 200 m to 0.1 J m^{-3} at about 4500 m. All the values for MKE are close to zero. The slightly increased value at 400 m ($n = 2$) is uncertain because of the shortness of the time series.

We now compare the energy terms from direct observations with those obtained from the model. During the first 100 days of model integration time the jet, which is initially almost completely zonal, develops meanders. During the following 200 days most of the flow is converted into an eddy field. The eddies have typical diameters of 100 to 200 km and translation velocities of about 0.02 m s^{-1} (see Plate 1).

In Figure 4 we present the distributions of the mean and the eddy kinetic energies in the cross-channel direction, averaged in time and over the length of the channel. The EKE has a maximum in layers 2 and 3, slightly south of the channel center at $y = 350$ km. Its value reaches 4.3 J m^{-3}. Compared to the fluctuating field, MKE has a relatively weak signal, with three local maxima in the upper layers at $y = 240$, 520, and 740 km and another maximum in layers 8 and 9 at $y = 400$ km. Thus the initially central jet has developed into separate ribbons, the positions of which may be explained in terms of the limited width of the unstable region [see *Onken and Klein*, 1991]. In

Table 3. Current Meter Record Statistics of Moored Array W3, W3.5, and W5

Mooring	Instrument	Depth, m	$\bar{u}$, 10^{-2} m s^{-1}	$\bar{v}$, 10^{-2} m s^{-1}	$\overline{u'^2}$, 10^{-3} m^2 s^{-2}	$\overline{v'^2}$, 10^{-3} m^2 s^{-2}	$\overline{u'v'}$, 10^{-3} m^2 s^{-2}	EKE, J m^{-3}	MKE, J m^{-3}
W3	1	205	−1.6 ± 10.0	−0.8 ± 12.4	2.50	3.87	−0.09	3.28	0.16
W3	2	410	−2.6 ± 9.0	0.8 ± 8.4	2.03	1.78	−0.68	1.96	0.38
W3	3	610	0.3 ± 7.4	−0.4 ± 7.0	1.33	1.21	−0.21	1.31	0.01
W3	4	1250	−1.0 ± 3.6	−0.3 ± 3.4	0.33	0.28	−0.07	0.31	0.06
W3	5	4775	−0.4 ± 1.6	−0.4 ± 2.2	0.06	0.13	0.03	0.10	0.01
W3.5	1	150	0.9 ± 10.8	0.2 ± 13.4	2.93	4.52	−0.92	3.84	0.04
W3.5	2	350	−0.7 ± 5.6	0.4 ± 8.2	0.80	1.69	−0.60	1.28	0.04
W3.5	3	575	0.9 ± 5.2	−0.0 ± 5.8	0.66	0.86	−0.13	0.78	0.04
W3.5	4	1200	−0.5 ± 3.6	−0.4 ± 4.0	0.33	0.40	−0.15	0.37	0.02
W3.5	5	4920	−0.1 ± 0.8	0.2 ± 1.2	0.02	0.04	0.00	0.03	0.00
W5	2	330	−1.9 ± 10.4	−0.6 ± 7.4	2.72	1.39	−0.03	2.11	0.21
W5	3	570	−0.7 ± 6.8	−0.3 ± 5.6	1.16	0.78	0.15	1.00	0.03
W5	4	1245	−1.0 ± 4.8	−0.6 ± 4.0	0.59	0.38	−0.07	0.50	0.08
W5	5	4570	−0.3 ± 1.2	−0.5 ± 0.8	0.03	0.09	0.02	0.06	0.02

See text, section 2 for definitions. Ranges for $\bar{u}$, $\bar{v}$ are valid for 95% confidence limit.

the upper layers the MKE maximum at y = 520 km is approximately located at the initial position of the jet, whereas the maxima at y = 240 and 740 km are due to anticyclonic and cyclonic eddies that have been pinched off to the south and the north, respectively, and their further meridional translation is prohibited by the planetary vorticity gradient. The maximum MKE values of 1.8 J m^{-3} found in layers 2 and 3 are lower by a factor of about 2.4 compared with those of the eddy kinetic energy.

A further averaging of these cross-channel/depth distributions over a 800-km-wide centered strip of channel width (to eliminate boundary influences) leads to the profile of EKE versus mean layer depth in Figure 5. A distinct maximum reaching values of about 2 J m^{-3} is found at a mean layer depth of 50–60 m. Near 500 m the vertical gradient is reduced. The corresponding values from the moored current meter records are also given in Figure 5. For great depths (1200 and 4500 m) a good correspondence is found between model and mooring values. At 600 m, however, the mooring values are higher by a factor of about 2. This ratio increases to 3 at the uppermost two instrument levels. In summary, the vertical distribution of EKE versus depth in the model is similar to that of the observations and the values agree quantitatively within a factor of 2–3.

Comparing the ratio EKE:MKE from the space-time averages in the model to those from the mooring, we find that it varies between about 4:1 and 5.5:1 in the model, thus being considerably smaller than the ratio found in the moorings where EKE exceeds MKE by 1 to 2 orders of magnitude. This underestimation of EKE is a feature found in many other numerical models. The good qualitative agreement of the distribution in model and observation, however, encourages us to assume that the energy transfer terms that we derive from the model are a good representation of the real processes.

6. Energy Transfer Terms

6.1. Basin Mean Distribution

We first show the time series of basin-wide-averaged energy transfer terms in Figure 6. All of them start growing from zero, and after about 100 days of integration time they reach values comparable to those encountered during the rest of the model run.

Barotropic instability processes, represented by c(MKE,EKE), appear to be relatively weak. This term is 1 order of magnitude smaller than the others. Obviously, it is not important for the development of disturbances from the mean current.

The highest values indicating a strong conversion from potential to kinetic energy are found around day 150. Later, the baroclinic instability term c(PE,EKE) approaches approximately 0.04 μW m^{-3} and c(PE,MKE) is found at values of −0.02 μW m^{-3}. This means that mean kinetic energy is converted to potential energy, while potential energy is transferred into eddy kinetic energy by baroclinic instability. As a consequence, the net conversion from potential to kinetic energy c(PE,KE) as its residuum is lower, with values near 0.02 μW m^{-3}. Potential energy is transferred into kinetic energy almost all the time; the mean circulation is reduced while the fluctuations are amplified. We thus find a regime that essentially has a balance with a high EKE to MKE ratio.

For completeness, we have also added the basin-wide energy dissipation D to Figure 6. During the first 170 days the absolute value increased monotonically from zero to somewhat more

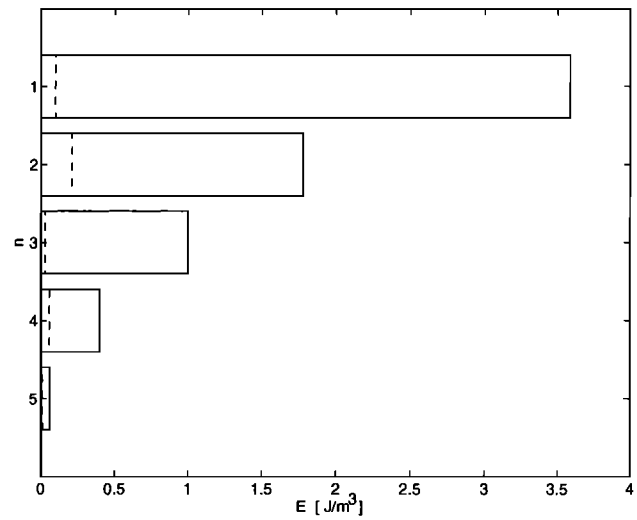

Figure 3. Kinetic energy terms E of the mooring array (W3, W3.5, and W5). Values are averages of all instruments at the respective level. Solid lines represent eddy kinetic energy (EKE); dashed lines are mean kinetic energy (MKE), and n is instrument number (see Table 3).

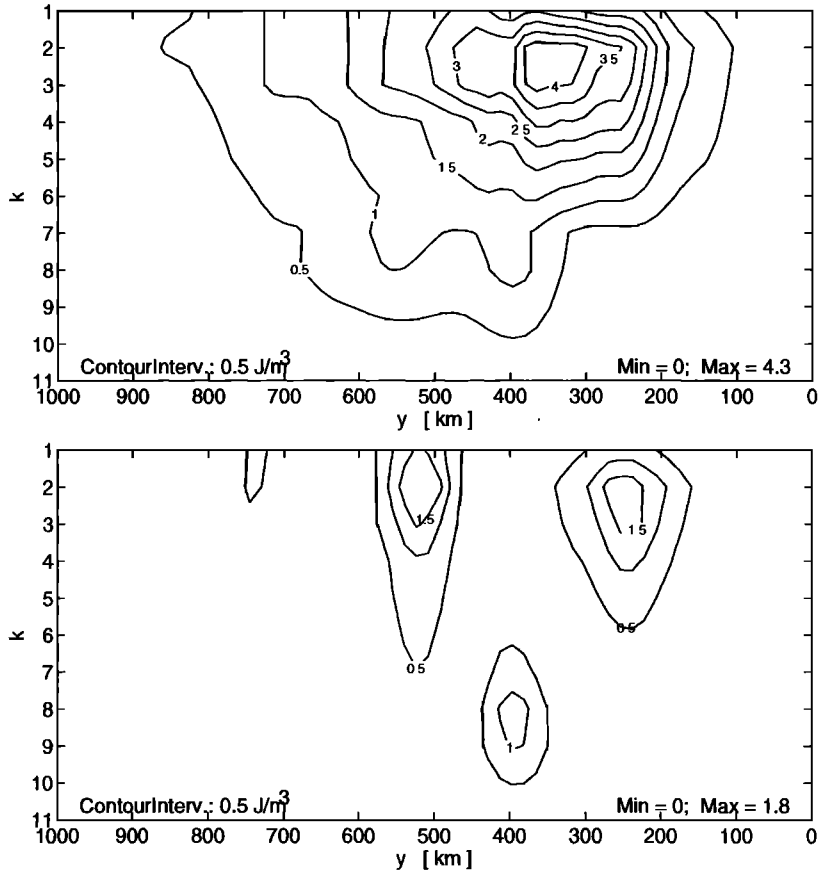

Figure 4. Cross-channel section of (top) EKE and (bottom) MKE, averaged in time and over the length of the channel. Here k is the number of the level.

than 0.04 μW m^{-3}, and afterward, it continued fluctuating around this level which is comparable in magnitude to the other conversions. Hence a significant fraction of the net gain of kinetic energy c(PE,KE) is dissipated and the system moves toward a marginally stable state. This is confirmed also by the temporal evolution of the eddy kinetic energy (not shown) which starts from zero and reaches 50% of its final (day 700) value after about 200 days. It is also worth mentioning that the apparent convergence of all conversion terms around zero at the end of the model run is just an artifact of the model time limit. In an extra model run up to day 1000, both c(PE,EKE) and c(PE,KE) continued oscillating between about -0.01 and 0.04 μW m^{-3}. The decreasing trend of all conversions is obviously due to the depletion of the reservoir of available potential energy and dissipation.

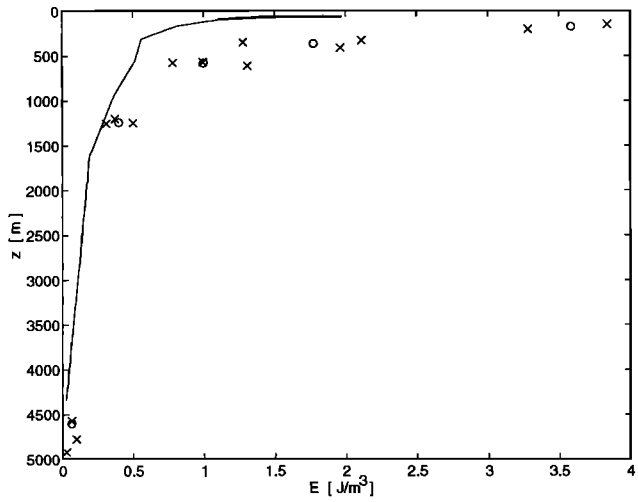

Figure 5. Profile of EKE averaged in the y direction (solid line) versus mean density layer depth z. Crosses denote EKE of the single instruments; circles are the mean EKE of the total moored array.

6.2. Cross-Frontal Distribution

In Figure 7 we present the cross-channel distribution of the zonally averaged baroclinic conversion term C(PE,EKE). A wavelike structure can be observed, with a maximum of 40 μW m^{-3}. To the north the amplitude decreases quickly, while two distinct local extrema exist in the south, reaching values of -26 and 20 μW m^{-3}, respectively.

The corresponding distribution of C(PE,MKE) has a similar structure, with smaller amplitude and opposite sign. Local extrema are found at the same locations as those of C(PE,EKE). Thus, at locations where the growth of fluctuations by baroclinic instability is strong, the largest amounts of energy are taken from the mean current and are converted to potential energy. Therefore the total conversion of energy has essentially the same structure as the baroclinic instability conversion.

6.3. Vertical Distributions

Averaging the distributions in the cross-channel y direction over a central channel width of 800 km (100 km $< y <$ 900 km)

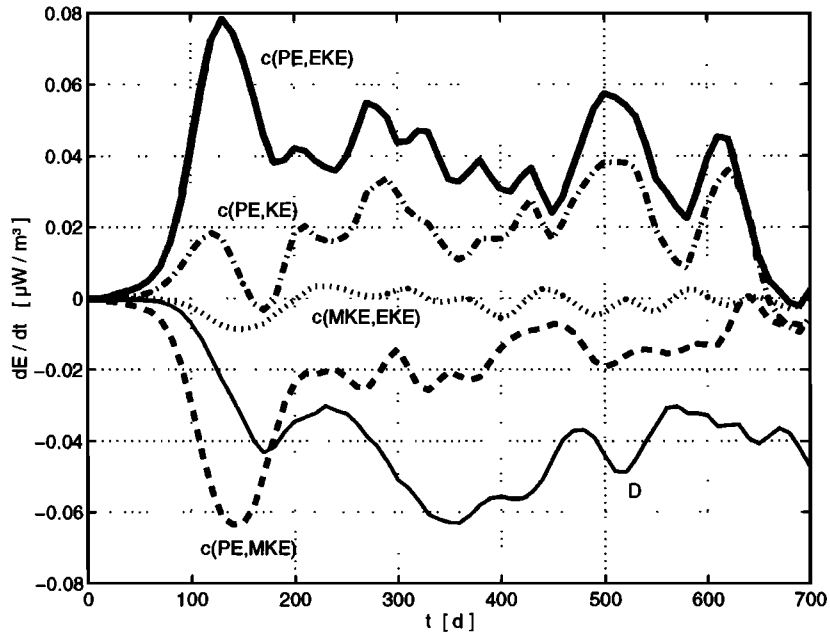

Figure 6. Total basin energy transfers versus time. Thick solid line denotes c(PE,EKE), dashed line is c(PE,MKE), dash-dotted line is c(PE,KE), dotted line is c(MKE,EKE), and thin solid line is viscous dissipation D.

leads to the profiles of the conversion terms with density (depth) for the upper 600 m presented in Figure 8.

Again, the concentration of high values of all terms in the upper layers can be clearly seen. The essential parts of all conversion terms are found in the upper 300 m of the water column. Maximum absolute values of C(PE,EKE) and C(PE,MKE) are encountered in the depth range of 50 to 100 m. The baroclinic term reaches a maximum value of 2.7 μW m^{-3}, which must be balanced by a value of C(PE,MKE) of -1.9 μW m^{-3}. This results in a total conversion from potential to kinetic energy of C(PE,KE) = 0.8 μW m^{-3}. This term is positive throughout the whole water column. As stated previ-

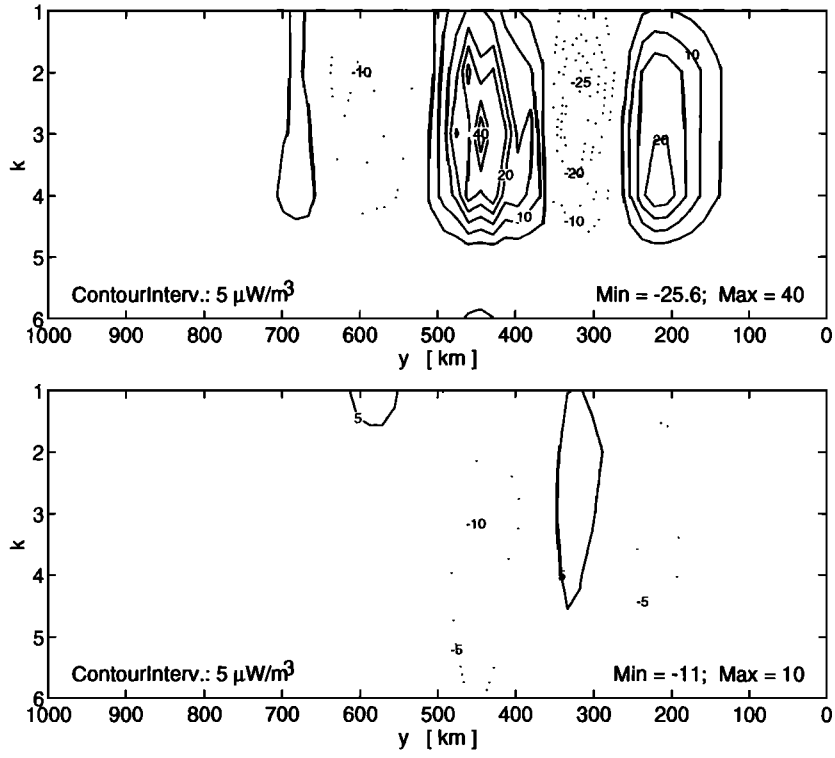

Figure 7. Cross-channel section of (top) C(PE,EKE) and (bottom) C(PE,MKE) zonally averaged over the channel length. Here k is the number of the level.

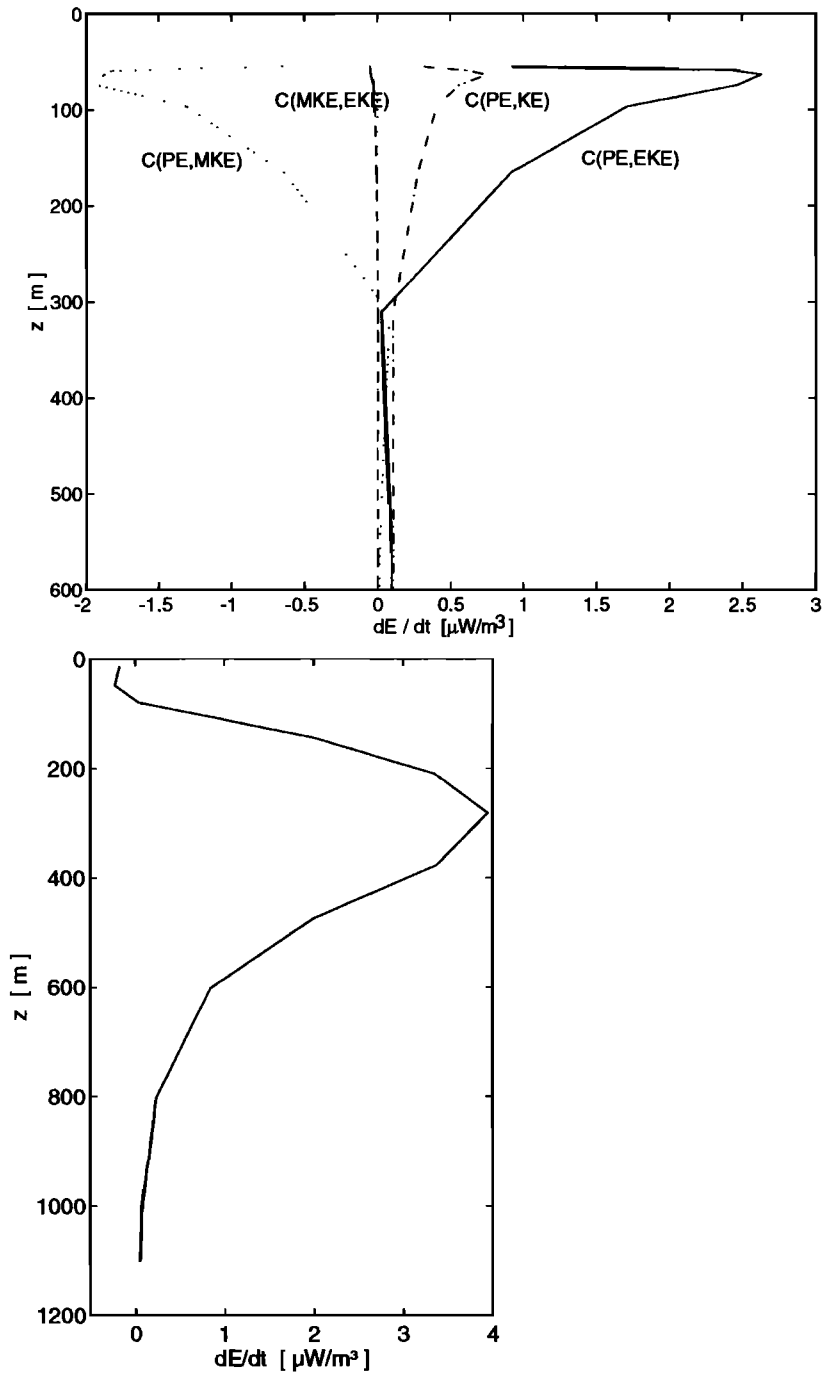

Figure 8. (top) Depth profiles of the transfer terms C(PE,EKE) (solid line), C(PE,MKE) (dotted line), C(PE,KE) (dash-dotted line), and C(MKE,EKE) (dashed line) for the upper 600 m of mean layer depths. Units are μW m^{-3}. (bottom) Depth profile of C(PE,EKE) as reconstructed from *Lindow* [1991] (see text). Units are μW m^{-3}. Note the different scales of the two profiles.

ously, the barotropic instability term of energy conversion, C(MKE,EKE), is of minor importance and close to zero in relation to the remaining terms.

6.4. Temporal Changes of Conversion Terms

Strong averaging of the conversion terms in time and/or space provided an overview of the magnitudes and made the results comparable to observations. On the other hand, information that may be useful for understanding how the system works is lost in this process. In order to provide this information, we present the energy conversion terms in their evolution in time.

First, we present time series of layer averages, with averaging again done over a 800-km-wide zonal strip. Figure 9 includes the time series of the conversion terms in layers 3, 6, and 9 over the total 700-day model run. As in the basin-averaged time series, the curves show an almost synchronous variation of c(PE,EKE) and c(PE,MKE), with opposite sign in all layers. This, in turn, leads to lower values for c(PE,KE). The term of

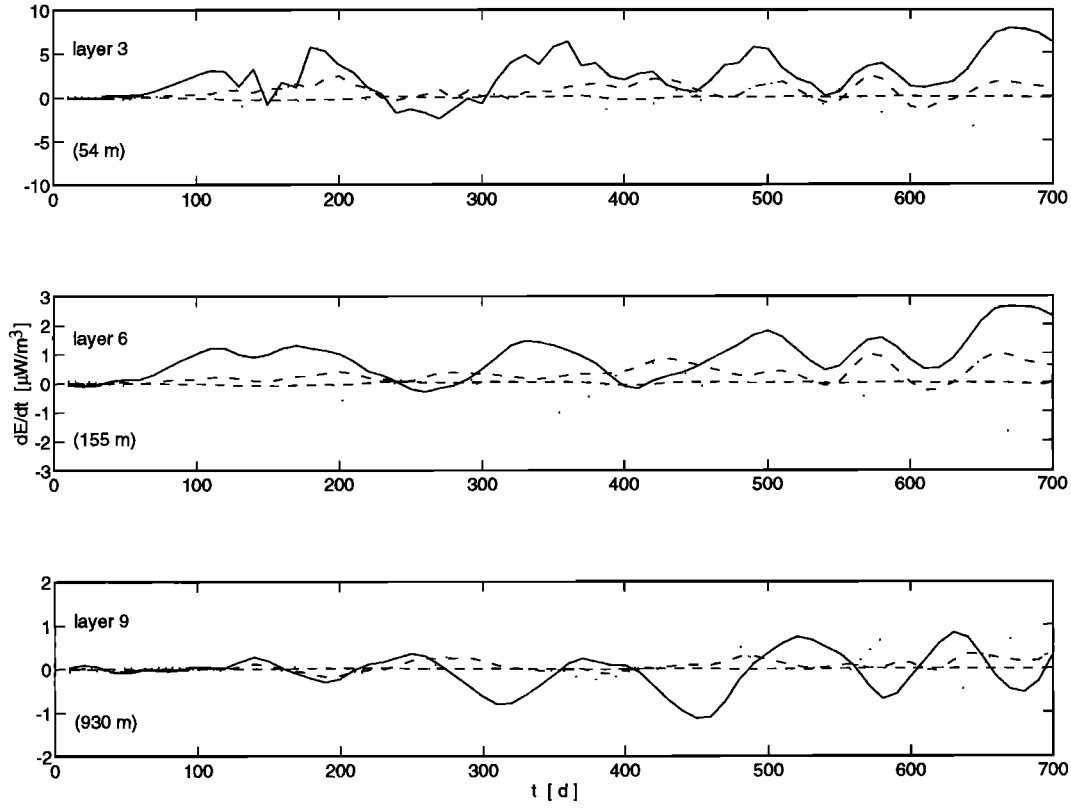

Figure 9. Time series of layer mean energy conversion terms in layers 3, 6, and 9. Solid lines are c(PE,EKE); dotted lines are c(PE,MKE); dash-dotted lines are c(PE,KE); and dashed lines are c(MKE,EKE). The values at left are the respective mean layer depth.

barotropic instability is again found to be negligible. The amplitudes of the variations, however, are much larger than the related average values (see Figure 8). In layer 3, with a mean depth of 54 m, the difference corresponds to a factor of 2–3. In the deeper layers it increases to 1 order of magnitude. Peak values of c(PE,EKE) and c(PE,MKE) are of order 10 μW m^{-3} in layer 3. Here these terms balance better than the time/layer means. The oscillations of the energy conversion terms are due to the fact that in nonlinear systems, unstable waves vacillate. That is, they do not grow continuously; after a period of wave growth comes a reduction in wave amplitude, which is followed by another growth cycle [*Hide and Mason*, 1975].

For a check on the spatial distribution of conversion terms, Plate 1 shows a snapshot of c(PE,EKE) and c(PE,MKE) in layer 3 at model day 380. The (horizontally even stronger) correlation of the two terms is eye catching. Almost everywhere, c(PE,EKE) has the same magnitude and the opposite sign as c(PE,MKE). Only the small differences in absolute values between the two terms lead to low values of c(PE,KE). The absolute values of the conversion terms are thereby much greater than the layer means; while c(PE,EKE) has a horizontal mean of 4.2 μW m^{-3}, local values are varying between -840 and $+860$ μW m^{-3}. Values of c(PE,MKE) are between -790 and $+770$ μW m^{-3}, adding up to a mean value of -3.6 μW m^{-3}. The difference between mean and local values can thus reach at least 2 orders of magnitude. In the present example we find the strongest signals of the conversion terms at the five eddies located between 200 km $< y <$ 600 km, centered at x = 100, 250, 350, 550, and 800 km. All these eddies move mainly westward, except the one at x = 550 km, which moves in a more southwestward direction. Their translation velocity is about 0.02 m s^{-1}. The eddies at x = 100 and 350 km rotate in a cyclonic sense; the others rotate in an anticyclonic sense.

Regarding a transient cyclonic eddy as a perturbation moving through a more or less undisturbed field, one finds large positive values of c(PE,EKE) located at the forward side, with respect to the direction of eddy propagation, and large negative values in the back. The opposite is true for the anticyclonic eddies. The translation of the eddy results in a vertical displacement of isopycnals and a disturbance of the vertical velocity, $w' \neq 0$. This, together with the related values for u' and v' due to the equation of continuity, results in the distribution of the conversion terms shown in Plate 1 (see (5)–(8)). The patterns show the strong correlation between the transient eddy field and the distribution of the conversion terms. Also, the smaller scale of the transfer term fields in relation to the eddy field can be seen.

7. Conclusions

The purpose of this study is to provide new information on energy and energy transfer terms in the Cape Verde Frontal Zone, i.e., the transition between the southeastern subtropical North Atlantic and the eastern equatorial regime.

We compared kinetic and potential energy terms from noncoherent mooring observations and an isopycnic frontal model. The mooring data resulted in eddy kinetic energy values of 1.0–3.8 J m^{-3} in the upper 400 m, dominating the mean kinetic energy by 2 orders of magnitude. Earlier data from moorings

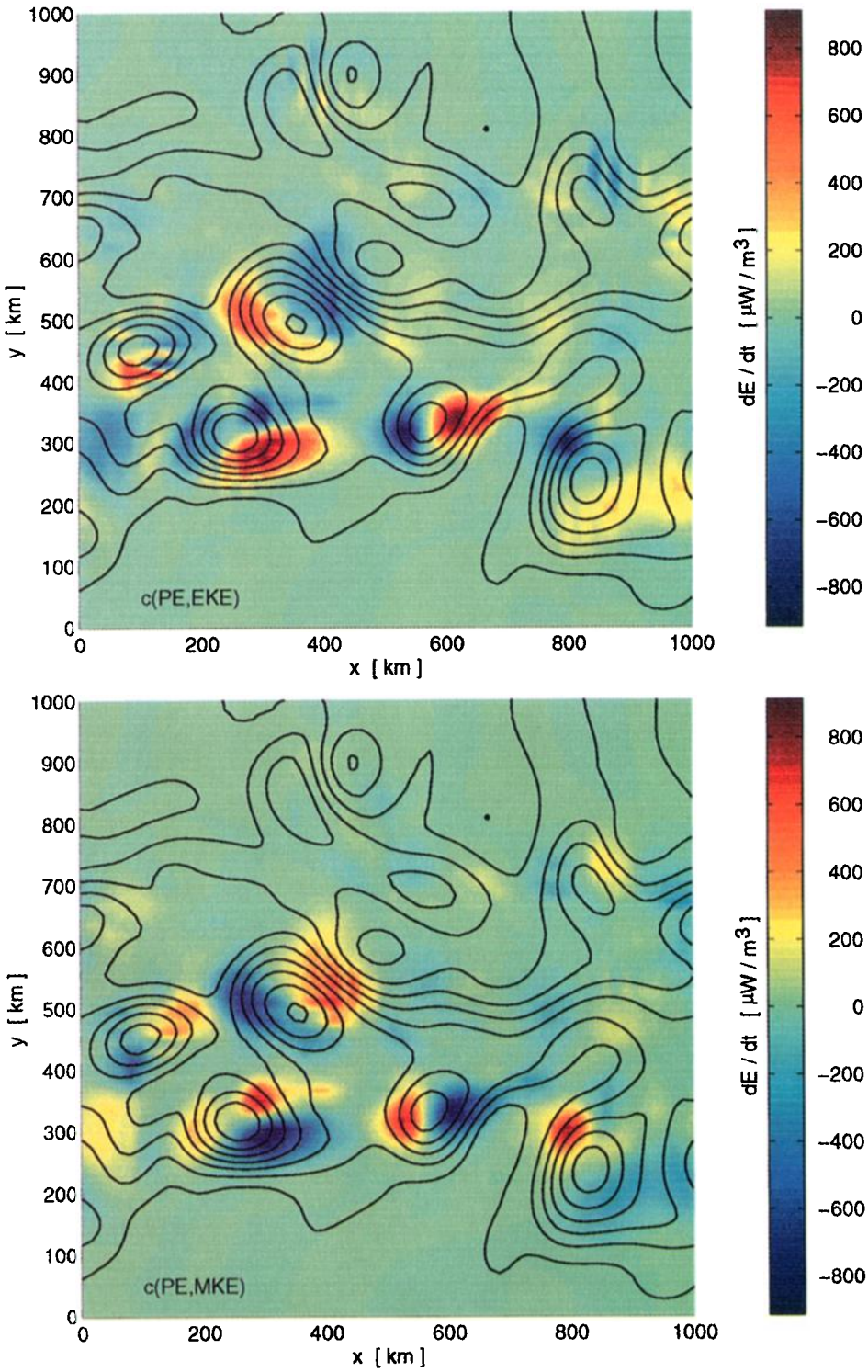

Plate 1. Energy conversion terms (top) c(PE,EKE) and (bottom) c(PE,MKE) in layer 3 on model day 380. Different colors represent magnitudes and signs of the terms. Units are μW m^{-3}. Overlying contours represent the streamfunction.

and SOFAR floats in the region have lead to similar values of eddy kinetic energy [see *Spall*, 1992; *Beckmann et al.*, 1994]. The corresponding energy terms from the model are lower by a factor of 2–3 in the upper layers compared with those of the observations. However, as we are able to show that the vertical distribution patterns of the energy terms are quite similar to observational and modeling results, we conclude that the behavior of energy transfer terms can also be expected to be similar.

The transfer term C(PE,EKE), describing the effect of baroclinic instability, was shown to be dominating in the frontal region. We found time-space means of 2–3 μW m^{-3} in the

pycnocline layers, varying with a standard deviation of 2.4 μW m^{-3} in the most active layer. Instantaneous values of layer means can reach 8 μW m^{-3}, and the zonally and time-averaged terms can amount up to about 40 μW m^{-3}. If we determine the spatial distribution of local energy transfer magnitudes, we find a strong correlation between it and the transient eddy pattern in the frontal flow, with areas of maximum transfer terms C(PE,EKE) up to about 1000 μW m^{-3}. The transfer term C(PE,MKE) has similar magnitudes and opposite sign, leading to small residual values for spatial means.

Lindow [1991] used a z coordinate North Atlantic circulation model with 1/3° resolution to determine such transfer terms. Averaging in time and zonally over 6°, she obtained a maximum C(PE,EKE) of 4 μW m^{-3} at a meridional section near 20°N (Figure 8). Although the magnitude is reasonably similar to our results, the spatial structure found here is poorly represented in her distributions. In Lindow's model with its lower resolution, the pycnocline is found at deeper levels and has a larger depth range, so, consequently, her conversion terms show a similar behavior. The results from *Spall* [1990] were also obtained by a z coordinate, large-scale circulation model. Averaging in time, over the upper 500 m vertically and from 40°W to 25°W zonally, he found a C(PE,EKE) value of 9 μW m^{-3} in the vicinity of the Cape Verde Frontal Zone. The value is somewhat larger than in this study.

The results of *Lindow* [1991] and *Spall* [1990] agree with ours in the respect that the barotropic instability term was much smaller than the remaining transfer terms. The low-velocity field and small horizontal shear are believed to be the cause of this. *Treguier* [1992] calculated the barotropic instability term in a z coordinate model with 1/3° resolution in latitude and 2/5° in longitude. The values are of similar magnitude to our results.

Although too low energy levels are produced by our and many other numerical models [cf. *Treguier*, 1992; *Beckmann et al.*, 1994], we have done two additional model runs in order to check the extent to which this might be caused by our model setup. In the first run we used a flat instead of a sloping bottom, and in the second run we doubled the horizontal resolution. Qualitatively, the results of all runs agreed among themselves, but in the flat bottom run the values for the energy conversions and the mean and eddy kinetic energy were lower. In contrast, refinement of the grid size led to an increase of the basin-wide energy conversion by about 10% and an eddy kinetic energy level that was about 50% higher than in the low-resolution run. We conclude that sufficient horizontal resolution far beyond the Rossby radius is essential for obtaining correct energy levels. Another reason for the still too low energies may be the general setup of our model transforming the real nonzonal mean flow of the Canary Current into a zonal flow with reduced β and superimposed by a perturbation, the wave vector of which is oriented parallel to the mean flow. According to *Spall* [1994], enhanced growth of unstable waves and a higher level of eddy kinetic energy may be expected in the case of a nonzonal mean flow perturbed by waves inclined to the mean flow direction. In addition, *Spall* [1990] suggested that conversion rates that are too low in the model may be partially responsible for low energy values. On the other hand, low eddy kinetic energy in the model also possibly implies an underestimation of the energy transferred, even if the ratio need not necessarily be the same. In a study of the Gulf Stream recirculation region, *Bryden* [1982] used data from the POLYGON Mid-Ocean Dynamics Experiment, Local Dynamics Experiment coherent mooring array to calculate a local value of EKE = 5.9 J m^{-3} for a 225-day period in a depth range of 600 to 850 m, along with a baroclinic transfer value of C(PE,EKE) = 3.3 μW m^{-3} and a barotropic value of C(MKE,EKE) = -1.5 μW m^{-3}. The energy term is larger than in our study, but the baroclinic transfer term is similar.

The present study also demonstrates that the selection of spatial and temporal averaging has a major influence on the magnitudes of transfer terms, because the horizontal distribution of active transfer regions is closely related to the structure of transient eddies.

Acknowledgments. The excellent assistance by the crew of the RV *Meteor* in obtaining the mooring data and the staff of the Marine Physics Department, Institut für Meereskunde Kiel, in the observations and data processing is acknowledged. This work was funded by the Deutsche Forschungsgemeinschaft (SFB 133).

References

Barton, E. D., Meanders, eddies and intrusions in the thermohaline front off Northwest Africa, *Oceanol. Acta*, *10*(3), 267–283, 1987.

Beckmann, A., C. W. Böning, C. Köberle, and J. Willebrand, Effects of increased horizontal resolution in a simulation of the North Atlantic, *J. Phys. Oceanogr.*, *24*, 326–344, 1994.

Bleck, R., Finite difference equations in generalized vertical coordinates, I, Total energy conservation, *Contrib. Atmos. Phys.*, *51*, 360–372, 1978.

Bleck, R., On the conversion between mean and eddy components of potential and kinetic energy in isentropic and isopycnal coordinates, *Dyn. Atmos. Oceans*, *9*, 17–37, 1985.

Bleck, R., and D. B. Boudra, Initial testing of a numerical model using a hybrid (quasi-isopycnic) vertical coordinate, *J. Phys. Oceanogr.*, *11*, 755–770, 1981.

Bleck, R., and D. B. Boudra, Wind-driven spin-up in eddy-resolving ocean models formulated in isopycnic and isobaric coordinates, *J. Geophys. Res.*, *91*, 7611–7621, 1986.

Boudra, D. B., R. Bleck, and F. Schott, A numerical model of instabilities of the Florida Current, *J. Mar. Res.*, *46*, 715–751, 1988.

Bryden, H. L., Sources of eddy energy in the Gulf Stream recirculation region, *J. Mar. Res.*, *40*, 1047–1068, 1982.

Cox, M. D., An eddy resolving numerical model of the ventilated thermocline, *J. Phys. Oceanogr.*, *15*, 1312–1324, 1985.

Emery, W. J., W. G. Lee, and L. Maagard, Geographical and seasonal distribution of Brunt-Väisälä frequency and Rossby radii in the North Pacific and North Atlantic, *J. Phys. Oceanogr.*, *14*, 294–316, 1984.

Fiekas, V., J. Elken, T. J. Müller, A. Aitsam, and W. Zenk, A view of the Canary Basin thermocline circulation in winter, *J. Geophys. Res.*, *97*, 12,495–12,510, 1992.

Harrison, D. E., and A. R. Robinson, Energy analysis of open regions of turbulent flows—Mean eddy energetics of a numerical ocean circulation experiment, *Dyn. Atmos. Oceans*, *2*, 185–211, 1978.

Hide, R., and P. J. Mason, Sloping convection in a rotating fluid, in *Advances in Physics*, vol. 24, pp. 47–100, Academic, San Diego, Calif., 1975.

Klein, B., and G. Siedler, Isopycnal and diapycnal mixing at the Cape Verde Frontal Zone, *J. Phys. Oceanogr.*, *25*, 1771–1787, 1995.

Lindow, H., Energetische Analysen in verschiedenen wirbelauflösenden Modellen des Nordatlantik, diploma thesis, Univ. of Kiel, Kiel, Germany, 1991.

Lorenz, E. N., Available potential energy and the maintenance of the general circulation, *Tellus*, *7*(2), 157–167, 1955.

Müller, T. J., and G. Siedler, Multi-year current time series in the eastern North Atlantic Ocean, *J. Mar. Res.*, *50*, 63–98, 1992.

Müller, T. J., G. Siedler, and W. Zenk, Forschungsschiff Meteor, Reise Nr. 6, Atlantik 87/88, Fahrtabschnitte 1-3, Oktober-Dezember 1987, *Rep. 194*, Inst. für Meereskunde, Kiel, Germany, 1988.

Onken, R., and B. Klein, A model of baroclinic instability and waves between the ventilated gyre and the shadow zone of the North Atlantic Ocean, *J. Phys. Oceanogr.*, *21*, 53–67, 1991.

Oort, A. H., S. C. Ascher, S. Levitus, and J. P. Peixóto, New estimates

of the available potential energy in the World Ocean, *J. Geophys. Res.*, *94*, 3187–3200, 1989.

Orlanski, I., and M. D. Cox, Baroclinic instability in ocean currents, *Geophys. Fluid Dyn.*, *4*, 297–332, 1973.

Reid, J. L., B. A. Elliott, and D. B. Olson, Available potential energy: A clarification, *J. Phys. Oceanogr.*, *11*, 15–29, 1981.

Siedler, G., and R. Onken, Eastern recirculation, in *The Warmwatersphere of the North Atlantic Ocean*, edited by W. Krauss, pp. 339–364, Gebrüder Borntraeger, Berlin, 1996.

Siedler, G., H. Schmickler, T. J. Muller, H.-W. Schenke, and W. Zenk, Forschungsschiff Meteor, Reise Nr. 4, Kapverdenexpedition Oktober–Dezember 1986, *Rep. 173*, Inst. fur Meereskunde, Kiel, Germany, 1987.

Spall, M. A., Circulation in the Canary basin: A model/data analysis, *J. Geophys. Res.*, *95*, 9611–9628, 1990.

Spall, M. A., Rossby wave radiation in the Cape Verde Frontal Zone, *J. Phys. Oceanogr.*, *22*, 796–807, 1992.

Spall, M. A., Mechanism for low-frequency variability and salt flux in the Mediterranean salt tongue, *J. Geophys. Res.*, *99*, 10,121–10,129, 1994.

Spall, M. A., P. L. Richardson, and J. Price, Advection and eddy mixing in the Mediterranean salt tongue, *J. Mar. Res.*, *51*, 797–818, 1993.

Tomczak, M., An analysis of mixing in the frontal zone of South and North Atlantic Central Water off North-West Africa, *Prog. Oceanogr.*, *10*, 173–192, 1981.

Tomczak, M., Ausbreitung und Vermischung der Zentralwassermassen in den Tropengebieten der Ozeane, 1, Atlantischer Ozean, *Oceanol. Acta*, *7*(2), 145–158, 1984.

Tomczak, M., and P. Hughes, Three dimensional variability of water masses and currents in the Canary Current upwelling region, *Meteor Forschungsergeb.*, *A21*, 1–24, 1980.

Treguier, A. M., Kinetic energy analysis of an eddy resolving primitive equation model of the North Atlantic, *J. Geophys. Res.*, *97*, 687–701, 1992.

Zenk, W., T. J. Müller, and G. Wefer, Barlavento Expedition, Reise Nr. 9, 29. Dezember-17. März 1989, *Meteor Rep. 89-2*, Univ. of Hamburg, Hamburg, Germany, 1989.

Zenk, W., B. Klein, and M. Schröder, Cape Verde Frontal Zone, *Deep Sea Res.*, *38*, S505–S530, 1991.

W. Erasmi and G. Siedler, Abteilung Meeresphysik, Institut fur Meereskunde, Düsternbrooker Weg 20, 24105 Kiel, Germany. (e-mail: gsiedler@ifm.uni-kiel.de)

R. Onken, SACLANT Undersea Research Centre, Viale San Bartolomeo 400, 19138 La Spezia, Italy.

(Received April 8, 1997; revised February 12, 1998;
accepted April 17, 1998.)